Determination of the Maturity and Functionality of Tumor Vasculature by MRI: Correlation Between BOLD-MRI and DCE-MRI Using P792 in Experimental Fibrosarcoma Tumors

Christine Baudelet,[1,2] Gregory O. Cron,[1] and Bernard Gallez[1,2]*

Using hypercapnia and carbogen as functional markers of vessel maturation and function, we compared blood oxygen level-dependent (BOLD) contrast with standard dynamic contrast-enhanced (DCE)-MRI quantitative parameters in murine fibrosarcoma. Our results show that there was no correlation between vessel maturity and contrast-agent uptake rate (K^{Trans}_{in}) or contrast agent efflux rate (k_{ep}). In addition, DCE-MRI provided higher estimates of the fraction of functional tumor compared to BOLD-MRI. The two putative markers of regional vascular density, i.e., the magnitude of BOLD signal change during carbogen challenge (VF) and the fractional plasma volume found by DCE-MRI (V_p), were only weakly correlated (r^2 = 0.02–0.14). Furthermore, VF showed no correlation with K^{Trans}_{in}. A positive correlation was observed (r^2 = 0.75) between mean tumor VF and k_{ep}, but only when averaged over the whole tumor (which includes tumor regions completely unperfused by the gadolinium (Gd) contrast agent). This would merely reveal a relationship between perfusion status and the capacity to respond to carbogen breathing. In conclusion, characterizations of tumor microvasculature imaging using BOLD-MRI and DCE-MRI appear to be largely complementary, given the weak correlations between their corresponding derived parameters. Magn Reson Med 56:1041–1049, 2006. © 2006 Wiley-Liss, Inc.

Key words: tumor; DCE-MRI; BOLD-MRI; carbogen; vessel maturation; vessel permeability

Both blood oxygenation level-dependent (BOLD) (1) MRI and dynamic contrast enhanced (DCE) MRI have emerged as useful techniques for noninvasive imaging of tumor vasculature (2,3). BOLD-MRI has been used to study tumor vascular growth (4), hemodynamic changes in response to treatments (5–12), acute hypoxia (13), vessel maturation (14–17), and functional status of the vascular bed (14,15,18,19). DCE-MRI also provides important information regarding tumor function and anatomy. Parameters such as blood flow, capillary permeability, interstitial space, and blood volume can be determined by analyzing the kinetics of contrast-media uptake and wash-out (3,20,21).

Assessment of vessel maturation and function with BOLD- or DCE-MRI is an approach whose utility for cancer investigations is well recognized. However, few studies have examined these two techniques simultaneously on the same subject. Thus, our understanding of mechanisms that may relate BOLD- and DCE-MRI remains relatively underdeveloped. Among the few investigators who have focused on this issue, Rijpkema et al. (22) compared BOLD-MRI (response to 98%O_2/2%CO_2 gas) and DCE-MRI in meningioma patients. In their study, changes in T_2^* were found to correlate inversely with the wash-out rate of the Gd contrast agent. In two other papers, Peller et al. (23) and Jiang et al. (24) found no relationship between BOLD- and DCE-MRI. However, the latter two studies employed semi-quantitative DCE-MRI analyses instead of pharmacokinetic modeling. Although the reported parameters (maximum rate of enhancement and peak enhancement) may be related to physiological parameters, their lack of clear physiological significance could make their interpretation difficult (25).

In this study we compared BOLD-MRI measurement of vessel maturation (using hypercapnia, i.e., elevated levels of CO_2) and BOLD-MRI measurement of vessel functionality (using carbogen breathing, i.e., elevated levels of O_2 and CO_2) with DCE-MRI using standardized pharmacokinetic quantities (25).

DCE-MRI measurement of uptake and wash-out of a contrast agent can help to characterize vasculature during the neoangiogenesis process (20). In this study we assessed how these parameters correlated with BOLD-MRI measurements of neovascular maturation and function. Furthermore, we assessed regional tumor blood volume using DCE-MRI, by estimating the fractional plasma volume. We used BOLD-MRI to obtain information about the regional blood volume by analyzing the magnitude of BOLD changes during carbogen breathing (26). We also compared both markers of vascular density.

MATERIALS AND METHODS

Animal Model

Syngeneic FSa-II fibrosarcomas were inoculated into the hind leg muscle of male C3H/HeOuJIco mice. MRI measurements were performed when tumors reached 8 ± 1 mm in diameter (8–9 days later). FSa-II tumors grow rapidly and are characterized by high vascular density,

[1]Laboratory of Biomedical Magnetic Resonance, Université Catholique de Louvain, Brussels, Belgium.

[2]Laboratory of Medicinal Chemistry and Radiopharmacy, Université Catholique de Louvain, Brussels, Belgium.

Grant sponsor: Belgian National Fund for Scientific Research; Grant number: 7.4503.02; Grant sponsor: Fonds Joseph Maisin and Actions de Recherches Concertées, Communauté Française de Belgique; Grant number: ARC 04/09-317.

*Correspondence to: Professor Bernard Gallez, Laboratory of Biomedical Magnetic Resonance, Laboratory of Medicinal Chemistry and Radiopharmacy, Université Catholique de Louvain, E. Mounier Ave. 73.40, B-1200 Brussels, Belgium. E-mail: Gallez@cmfa.ucl.ac.be

Received 6 October 2005; revised 30 May 2006; accepted 10 July 2006.
DOI 10.1002/mrm.21047
Published online 19 September 2006 in Wiley InterScience (www.interscience.wiley.com).

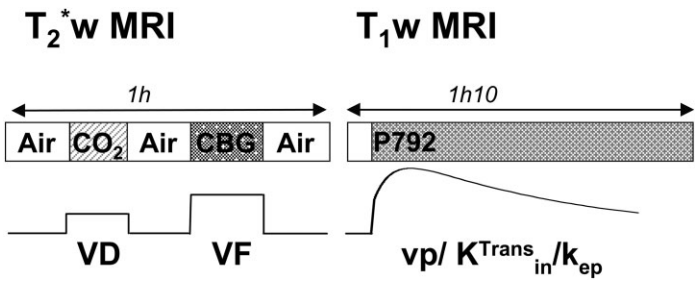

FIG. 1. Schematic of the MRI protocol and derived parameters.

heterogeneous distribution of functional vasculature, and a poor degree of vessel maturation (27). The mice were anesthetized with isoflurane 1.2% in air administered with a face mask. Anesthetized mice were placed prone and were immobilized with adhesive tape. Warm air was flushed into the magnet to maintain the body temperature at 37°C.

MRI

MRI was performed with a 4.7-Tesla (200 MHz, ^{1}H) 40-cm inner-diameter bore system (Bruker Biospec, Ettlingen, Germany). The mice were positioned into a 70-mm inner-diameter birdcage radiofrequency (RF) coil. T_2-weighted (T_2w) anatomical images were acquired using a fast spin-echo (FSE) sequence (repetition time (TR) = 3 s, effective echo time (TE) = 63 ms). A 1.6-mm-thick slice was prescribed through the tumor center and was imaged first with BOLD-MRI and then with DCE-MRI (see Fig. 1).

BOLD-MRI

For BOLD-MRI we employed a T_2^*w gradient-echo (GRE) sequence with the following parameters: TR = 200 ms, TE = 18 ms, flip angle = 45°, receiver bandwidth = 12.5 kHz, 64 phase- and frequency-encode steps, linear encoding order, 4 cm field of view (FOV), two averages, and 25.6 s/image. A run of 140 sequential images was acquired. Maturation and functionality of the tumor vasculature were determined from the GRE images acquired during inhalation of air (first 20 scans), air containing 5% CO_2 (next 30 scans), air again (30 scans), carbogen (95% O_2, 5% CO_2, 30 scans), and finally air again (last 20 scans; Fig. 1, left schematic).

DCE-MRI

T_1w GRE images were obtained with the following parameters: TR = 40 ms, TE = 4.9 ms, slice thickness = 1.6 mm, flip angle = 90°, matrix = 64 × 64, FOV = 4 cm, receiver bandwidth = 25 kHz, resulting in an acquisition time of 2.56 s per scan. The T_1w images were of high quality with uniform signal intensity (SI) and contrast. The RF excitation field was assumed to be homogeneous throughout the tumor. The contrast agent was a rapid-clearance blood pool agent, P792 (Vistarem®; Laboratoire Guerbet, Aulnay sous Bois, France). P792 (MW: 6.47 kDa) is a monogadolinium macrocyclic compound based on a Gd-DOTA structure substituted by hydrophilic (dextran) arms. Its R_1 relaxivity in 37°C HSA, 4% at 4.7T is 9.0 $mM^{-1}s^{-1}$. P792 was injected at a dose of 0.042 mmol Gd/kg as recommended by the manufacturer and published studies (28). A proton density-weighted (PDw) image was acquired before DCE-MRI using the GRE sequence described above, but with the following parameters: TR = 8 s, TE = 4.9 ms, number of averages (NA) = 2. The DCE-MRI study was performed using the following protocol: After 12 baseline images were acquired, P792 was administered intravenously within 2 s (50 μl/40 g mouse) and the enhancement kinetics were continuously monitored for 8 min (200 total scans). This allowed us to sample the SI curve often enough to track the fast rise in tissue enhancement for viable tumor following bolus influx. Immediately after this, a slower DCE data set was acquired to monitor the washout of the contrast agent. For this second set, 60 scans were acquired at a temporal resolution of 60 s (24 averages, 1 hr total).

Data Analysis

MRI data were analyzed using in-house-developed programs written in Interactive Data Language (RSI, Boulder, CO, USA). MRI raw data were zero-filled and 2D Fourier transformed, resulting in an in-plane resolution of 128 × 128. A region of interest (ROI) encompassing the tumor was drawn manually on the T_2w anatomical image. Each voxel in this ROI was subsequently analyzed for both GRE runs. We estimated the tumor size by calculating the surface area of the ROI, which represents the largest tumor section.

Vessel Functionality and Vessel Maturation Maps

By means of statistical parametric mapping, we generated vascular functional and vascular maturation maps. Image regression analysis was performed using the general linear model (GLM) approach (29). The hemodynamic response under gas-mixture breathing was found to be modeled best by a ramped boxcar (gradual linear increase or decrease for four scans at each end of the boxcar), as opposed to a simple rectangular boxcar function. A set of discrete cosine functions (N = 2) was also included in the design matrix to model low-frequency confounds. Appropriate contrast weights were used to test the null hypothesis of no change in SI during inhalation of CO_2 or carbogen, which corresponds to zero amplitude of the boxcar waveform (the significance level α was set to 0.01). Voxels that showed no significant change in SI during carbogen breathing were excluded from further statistical analysis. To assess the maturity and functionality of vessels, we used the VD and VF parameters, defined as the negative of

the change in $1/T_2^*$ induced by hypercapnia (breathing elevated levels of CO_2) or carbogen breathing, respectively. The parameter VD thus relates to vessel maturity, whereas VF relates to vessel functionality. The VD and VF depend on the changes in T_2^*w signal (as estimated using the regression analysis) and are calculated as follows (17):

$$VD \text{ or } VF = -\Delta R_2^* = \ln(SI_{pre}/(SI_{pre} + \Delta SI))/TE, \quad [1]$$

where SI_{pre} is the SI during normal-air breathing, ΔSI is the change in SI induced by CO_2 or carbogen breathing (when found statistically significant), and ΔR_2^* is the induced change in $1/T_2^*$. ΔR_2^* is a parameter that is proportional to the change in deoxyhemoglobin content, independently of native tissue T_2^* (in contrast to ΔT_2^*). VD and VF are thus also independent of native tissue T_2^*. Positive values are related to a decrease in deoxyHb content, e.g., when blood vessel oxygenation improves. VD was only estimated when VF was found to be significant. Because carbogen has a 5% CO_2 component, response to hypercapnia (5% CO_2) was considered to be a repeated event when carbogen was breathed. We calculated the fraction of functional tumor area (vascular functional index (VFI)) by dividing the number of tumor voxels with significant values for VF by the total number of tumor voxels.

Linear regression analysis was performed to assess the correlation between the different indices. A *t*-test was used to determine the significance of the correlation coefficient.

V_p, $K^{Trans}{}_{in}$, and k_{ep} Maps

We analyzed the total tumor ROI (which was drawn on the T_2w anatomical image) on a voxel-by-voxel basis to obtain parametric maps. Voxels that showed either no signal enhancement or a linear increase of SI were excluded from the analysis. This was achieved by identifying voxels with statistically significant variations in T_1w SI using a power spectrum analysis. Using cluster analysis (8), voxels for which typical signal enhancement curves were observed were then selected for pharmacokinetic analysis. Contrast-agent concentration as a function of time after P792 injection ($C(t)$) was estimated using the following equation:

$$C(t) = \left(\frac{1}{TR \cdot r_1}\right) \ln\left[\left(1 - \frac{S0_{T1w}}{S0_{PD}}\right)/\left(1 - \frac{S(t)}{S0_{PD}}\right)\right], \quad [2]$$

where TR is the repetition time of the T_{1w} image, r_1 is the relaxivity of the contrast agent (9.0 $mM^{-1}s^{-1}$), $S0_{T1w}$ is the preinjection SI for the T_1w image, $S0_{PD}$ is the preinjection SI for the PDw image, and $S(t)$ is the signal as a function of time after injection for the T_1w image. The tracer concentration changes were fitted to a two-compartment pharmacokinetic model as previously described (13,25).

The following equation describes the tissue concentration as a function of time:

$$C(t > t0) = K_{in}{}^{Trans} A0, \frac{\exp^{-\frac{K_{out}{}^{Trans}}{v_e}t} - \exp^{-klt}}{K1 - \frac{K_{out}{}^{Trans}}{v_e}} + v_p \cdot A0 \cdot \exp^{-klt}, \quad [3]$$

where $K^{Trans}{}_{in}$ is the influx volume transfer constant (into EES from plasma), $K^{Trans}{}_{out}$ is the efflux volume transfer constant (from EES back to plasma), V_e is the volume of EES per unit volume of tissue, and V_p is the blood plasma volume per unit volume of tissue. $K^{Trans}{}_{out}$ and V_e cannot be estimated separately, so only k_{ep}, the ratio $K^{Trans}{}_{out}/V_e$, is reported. k_{ep} is the fractional rate of efflux from the interstitial space back to the blood. The constants used in the fitting are the maximum concentration of P792 in the plasma ($A0$), the blood decay rate ($k1$), and the time to the maximum tracer plasma concentration ($t0$). It is assumed that the rapid enhancement phase (from $t = 0$ to $t0$) is primarily due to intravascular contrast media during the first pass of the contrast media bolus, while the slower phase is due to leakage into the extracellular space. The parameters $A0$, $k1$, and $t0$ were estimated from the enhancement kinetics in one or two selected renal cortex voxels (from an additional DCE-MRI slice prescribed on the kidneys) that showed early and large contrast agent signal enhancement, presumably reflecting pronounced arterial perfusion.

All fitting was performed using a Levenberg-Marquardt nonlinear least-squares procedure. Parametric images for V_p (a vascular volume-related parameter), $K^{Trans}{}_{in}$ (the influx volume transfer constant into extravascular-extracellular space from plasma), and k_{ep} (the fractional rate of efflux from the interstitial space back to the blood) were computed (only the statistically significant parameter estimates are displayed) (13). Statistical significance for V_p or $K^{trans}{}_{in}$ identified "perfused" pixels (i.e., pixels to which the contrast agent P792 had access). The fraction of perfused tumor was therefore defined as the number of voxels with statistical significance for V_p or $K^{trans}{}_{in}$ divided by the total number of voxels in the whole-tumor ROI. Significance for V_p alone (and not for $K^{trans}{}_{in}$) may theoretically occur in the case of voxels containing blood vessels that are impermeable to the contrast agent. However, in practice, we observed no such voxels. The fraction of perfused tumor is thus restrained to the percentage of voxels with contrast-agent uptake.

Analysis of the Relationship Between BOLD- and DCE-Derived Parameters

Within-Tumor Analysis

Figure 2 shows how tumors voxels should be distributed theoretically, depending on whether the parameters are found to be statistically significant. For both VD and VF, four groups of voxels may be considered, each of which is described by defined vascular characteristics. The significance for VD reveals the maturity of vessel vasculature, the significance for VF reveals the vessel functionality (presence of erythrocyte flow), and the magnitude of VF relates to vessel density. The significance for $K^{Trans}{}_{in}$ indicates vessel functionality (flowing blood vessels enable Gd contrast-agent influx), and the magnitude of $K^{Trans}{}_{in}$ reflects the efficacy of tumor contrast-agent uptake.

Between-Tumor Analysis

For each tumor voxel we calculated a set of BOLD and DCE parameters (values were set to 0 when a parameter was

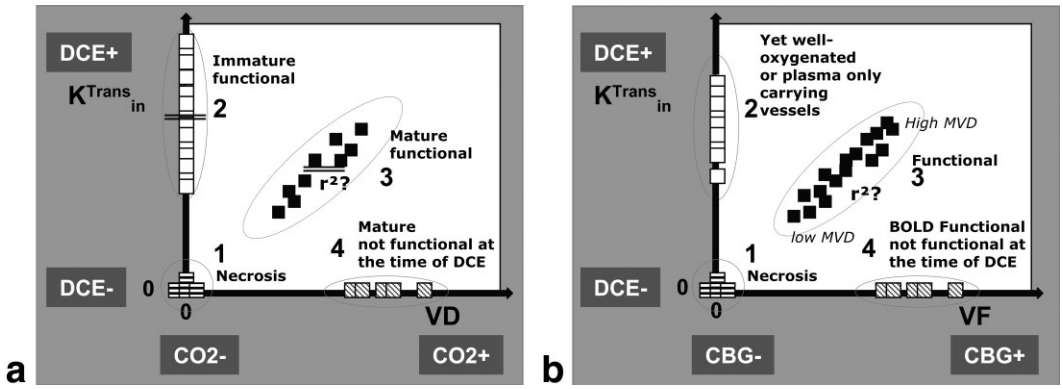

FIG. 2. Theoretical view on how tumor voxels would be distributed according to (**a**) their BOLD responsiveness to hypercapnia (CO_2+: VD significant, CO_2–: VD not significant) or (**b**) carbogen breathing (CBG+: VF significant, CBG–: VF not significant) and the Gd-based contrast agent influx during DCE-MRI (DCE+: K^{Trans}_{in} significant, DCE-: K^{Trans}_{in} not significant). Tumor voxels could be classified into four groups.

found to be nonsignificant). Whole-tumor averaged values of parameters were computed from these data. Correlations between these mean parameters for the seven tumors were tested for significance.

RESULTS

Relationship Between Hypercapnia-Induced BOLD Response and K^{Trans}_{in} or k_{ep}

Only 17% ± 2% (mean ± SEM) of tumor voxels responded to hypercapnia, indicating a low percentage of tumor regions containing mature vessels (Figs. 2a and 3a, groups 3 and 4 vs. groups 1 and 2). Of the voxels that did respond to hypercapnia, 78% ± 6% had significant values for K^{Trans}_{in} (Figs. 2a and 3a, group 3 vs. group 4). Tumor voxels with no response to hypercapnia and no significant K^{Trans}_{in} values represented 20% ± 6% of the tumor (Figs. 2a and 3a, group 1), revealing the necrotic part of the tumor.

We also compared the mean values of K^{Trans}_{in} and k_{ep} (only when found to be significant) between hypercapnia-responsive and -nonresponsive vessels (Fig. 2a, groups 2 and 3). No systematic significant difference in mean K^{Trans}_{in} values was observed between these two groups, nor was any systematic significant difference in k_{ep} observed (see Fig. 4a and b). K^{Trans}_{in} values were higher in tumor than in contralateral muscle (0.034 ± 0.004 vs. 0.011 ± 0.002 min^{-1}, whole tumor, and muscle ROIs, $P < .01$, paired *t*-test). However, k_{ep} values were the same in tumor and muscle (0.031 ± 0.004 and 0.029 ± 0.002 min^{-1}, respectively; see also Fig. 4a and b, gray bars = muscle).

We also quantified the correlation between VD values (magnitude of the BOLD response to hypercapnia) and K^{Trans}_{in} or k_{ep}. The whole-tumor averaged analysis revealed a lack of correlation between the mean tumor VD and mean K^{Trans}_{in} values (Fig. 5a, Table 1). VD and k_{ep} were only weakly correlated ($P = .09$; Fig. 5c, Table 1). In individual tumors, no significant correlations between VD and K^{Trans}_{in} or k_{ep} were observed on a voxel-by-voxel basis (with r^2 ranging in the seven tumors from 0 to 0.11 for K^{Trans}_{in} and from 0 to 0.03 for k_{ep}; see Fig. 2, group 3).

Relationship Between Carbogen-Induced BOLD Response and K^{Trans}_{in} or k_{ep}

In this tumor model the VFI (fraction of all tumor pixels that responded to carbogen breathing) was 50% ± 4% (mean ± SEM, $N = 7$; Figs. 2b and 3b, groups 3 and 4 vs.

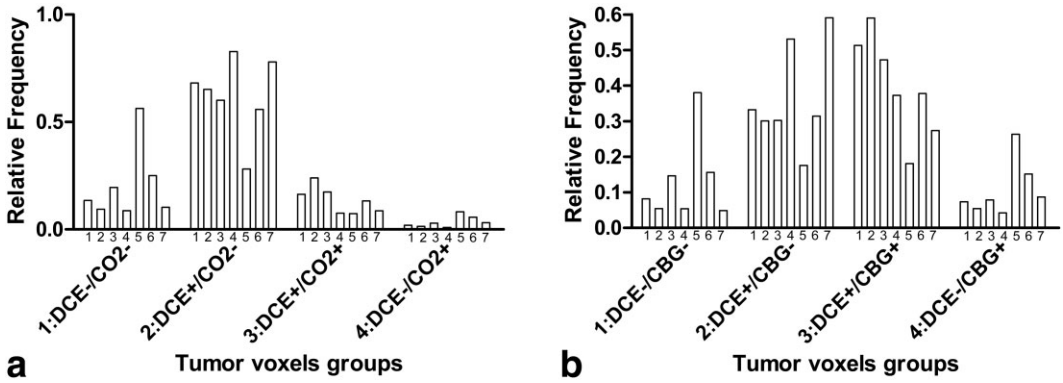

FIG. 3. Observed distribution of the tumor voxels as a function of tumor MR contrast-agent influx status (DCE+ vs. DCE–) and (**a**) BOLD responsiveness to hypercapnia (CO_2+ vs. CO_2–) or (**b**) to carbogen breathing (CBG+ vs. CBG–). Bars represent results for each individual mouse ($N = 7$).

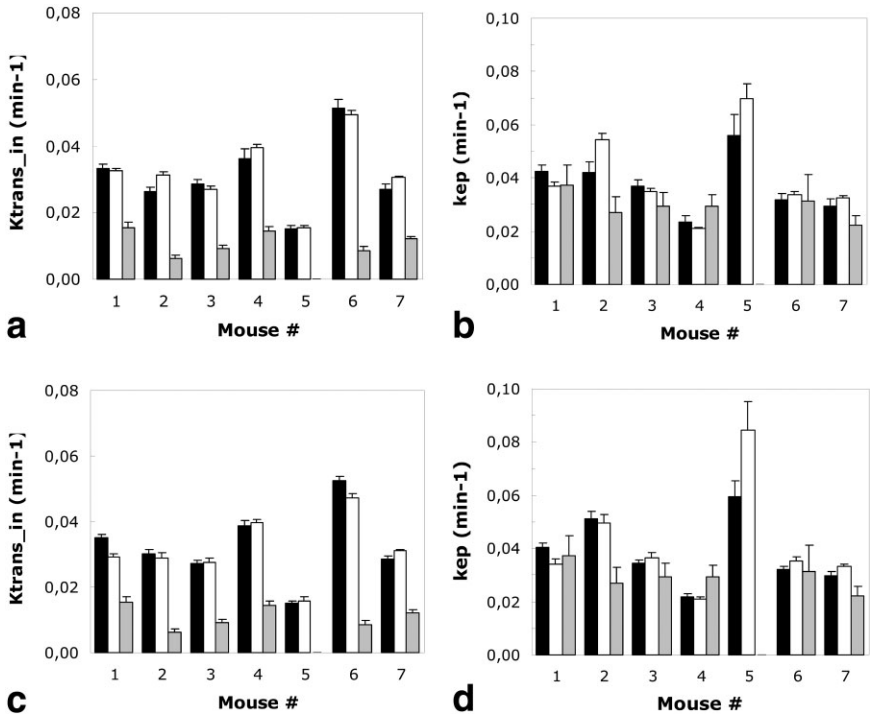

FIG. 4. **a:** Comparison of mean $K^{Trans}{}_{in}$ values for hypercapnia BOLD responsive voxels (black) and nonresponsive voxels (white). **b:** The same as a for a comparison of k_{ep} values. **c:** Comparison of mean $K^{Trans}{}_{in}$ values for carbogen BOLD responsive voxels (black) and nonresponsive voxels (white). **d:** The same as **c** for a comparison of k_{ep} values. Gray bars in plots are mean values of $K^{Trans}{}_{in}$ (a and c) or k_{ep} (b and d) observed in corresponding contralateral muscle. Data are the means ± SEM.

groups 1 and 2). The fraction (percentage) of tumor perfused by the Gd contrast agent was 76% ± 7%, which is significantly higher than the VFI ($P < .05$, paired *t*-test).

Of the tumor voxels that responded to carbogen breathing, 78% ± 7% were perfused by the Gd contrast agent (Figs. 2b and 3b, group 3). Of the tumor voxels that did not respond to carbogen breathing, 73% ± 8% were perfused by the Gd contrast agent (Figs. 2b and 3b, group 2). This indicates that carbogen reactivity is a poor discriminant factor for contrast-agent influx. The ratio between the two proportions (also called the relative risk (RR)) was small indeed (RR = 1.06, 95% CI = [1.02, 1.09]). This means that carbogen-responsive voxels were only 1.06 times more likely to also have a contrast-agent influx than carbogen-nonresponsive voxels. We also compared the mean values of $K^{Trans}{}_{in}$ and k_{ep} (averaged only over significant values) between carbogen-responsive and -nonresponsive vessels (Fig. 2b, groups 2 and 3). There was no systematic significant difference in $K^{Trans}{}_{in}$ or k_{ep} for these two groups (Fig. 4c and d).

We also performed a correlation analysis between VF and the $K^{Trans}{}_{in}$ or k_{ep} parameters. The whole-tumor averaged analysis revealed a lack of correlation between $K^{Trans}{}_{in}$ values and mean tumor VF (Fig. 5b). However, a significant positive correlation was observed between mean tumor VF and k_{ep} values ($r^2 = 0.75$, $P = .01$; Fig. 5d). Small values for VF in such tumors were not due to a lack of BOLD signal change during carbogen; rather, there was an equal proportion of negative and positive changes. For example, the mean absolute value of VF for mouse 7 was far from zero (Fig. 5f). Interestingly, the correlation between k_{ep} and VF was improved when the absolute value of VF was considered ($r^2 = 0.81$, $P = .005$; Fig. 5f). In addition, a significant positive correlation was observed between the VFI (percentage of tumor voxels responding to carbogen) and whole-tumor mean k_{ep} values ($r^2 = 0.66$, $P = .02$).

In individual tumors, no significant correlations between VF and $K^{Trans}{}_{in}$ or k_{ep} were observed on a voxel-by-voxel basis (with r^2 ranging in the seven tumors from 0 to 0.07 for $K^{Trans}{}_{in}$, and from 0 to 0.06 for k_{ep}; Fig. 2b, group 3). This is also demonstrated in the parametric maps in Fig. 6. For example, a lack of correlation between VF and $K^{Trans}{}_{in}$ is clearly visible in this figure. Zones of high VF values did not overlap with those of high $K^{Trans}{}_{in}$ values.

Relationship Between Hypercapnia and Carbogen-Induced BOLD Responses

The whole-tumor averaged analysis revealed a positive correlation between the mean VD and mean VF ($r^2 = 0.75$; Table 1). Tumors that demonstrated a mean negative VD were associated with low values for the mean VF (Fig. 5c and d). Similarly, the percentage of hypercapnia-responsive tumor voxels was strongly correlated with the VFI (percentage of carbogen responsive voxels; $r^2 = 0.82$, $P = .005$).

Relationship Between Carbogen-Induced BOLD Response and V_p

The estimated mean tumor fractional plasma volume as derived from P792 enhancement kinetics (V_p) was about 50% higher than in contralateral muscle tissue (V_p = 0.061 ± 0.005 vs. 0.040 ± 0.003, mean ± SEM, $P < .01$, paired *t*-test), reflecting the more pronounced vascular development in the tumor tissue. Both VF and V_p represent a measure of vascularity. The VF is determined by the mean perfused vascular fraction, whereas the V_p is related to blood volume (35). The whole-tumor averaged analysis

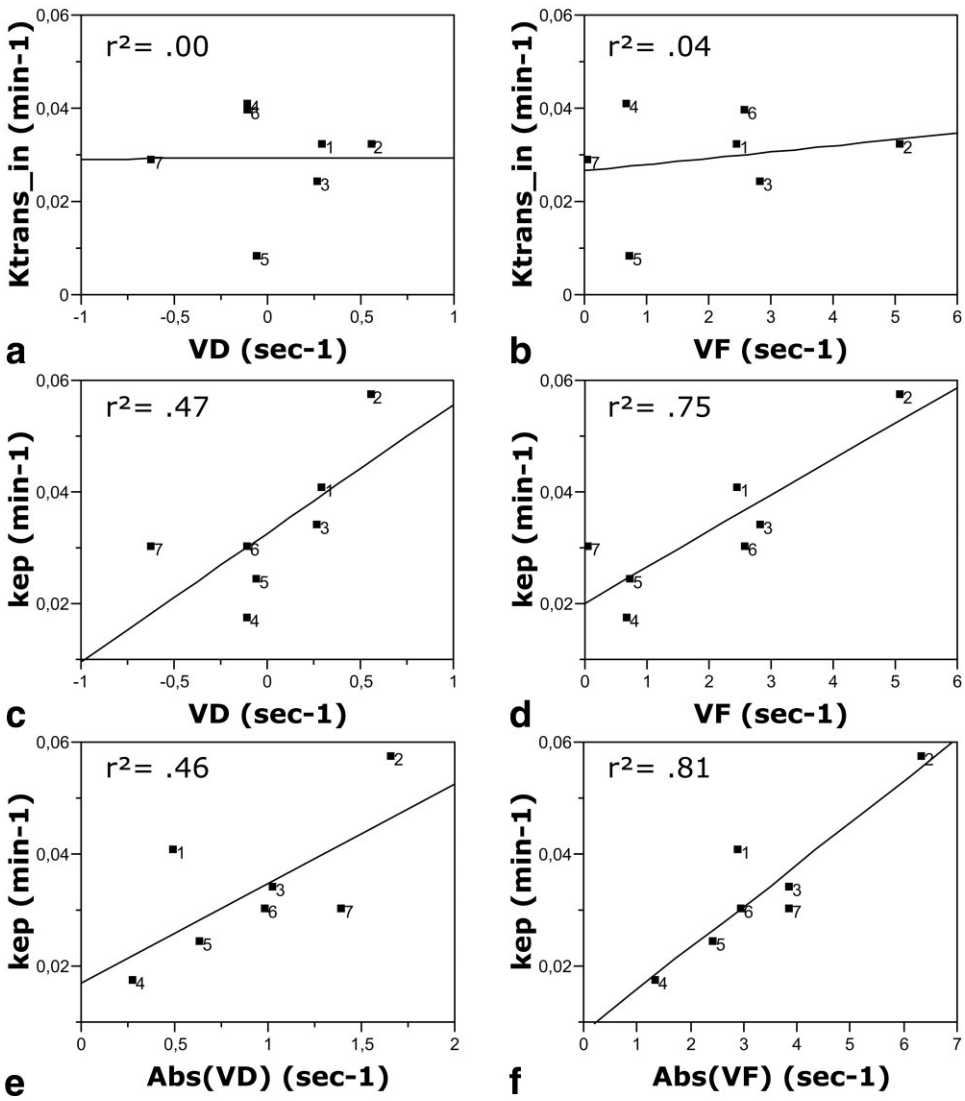

FIG. 5. Relationships between mean tumor DCE-MRI-derived parameters and VD or VF BOLD-MRI-derived parameters. Linear fit, r^2, and tumor labels are given.

Table1
Pairwise Correlations Between Whole Tumor Averaged BOLD and DCE Parameters

K^{Trans}_{in}							
+0.07	k_{ep}						
0.89							
–0.62	–0.09	Vp					
0.13	*0.84*						
+0.00	+0.69	+0.19	VD				
1.00	*0.09*	*0.68*					
+0.21	**+0.86**	–0.01	**+0.87**	VF			
0.65	*0.01*	*0.97*	*0.01*				
– 0.09	**+0.86**	+0.12	**+0.77**	**+0.92**	$\%CO_2+$		
0.85	*0.01*	*0.79*	*0.04*	*0.003*			
+0.14	**+0.81**	+0.06	**+0.92**	**+0.95**	**+0.91**	%CBG+	
0.76	*0.03*	*0.89*	*0.003*	*0.001*	*0.005*		
+0.78	+0.51	**–0.86**	+0.21	+0.43	+0.23	+0.34	%DCE+
0.04	*0.24*	*0.01*	*0.64*	*0.32*	*0.62*	*0.45*	

Data are Pearson correlation coefficient (calculated for seven tumors). Corresponding *P* values are italicized. Significant correlations are typed in bold. The % CO_2+ and % CBG+ parameters are the percentage of hypercapnia and carbogen responsive tumor voxels respectively. The % DCE+ parameter is the percentage of tumor voxels with contrast agent entry.

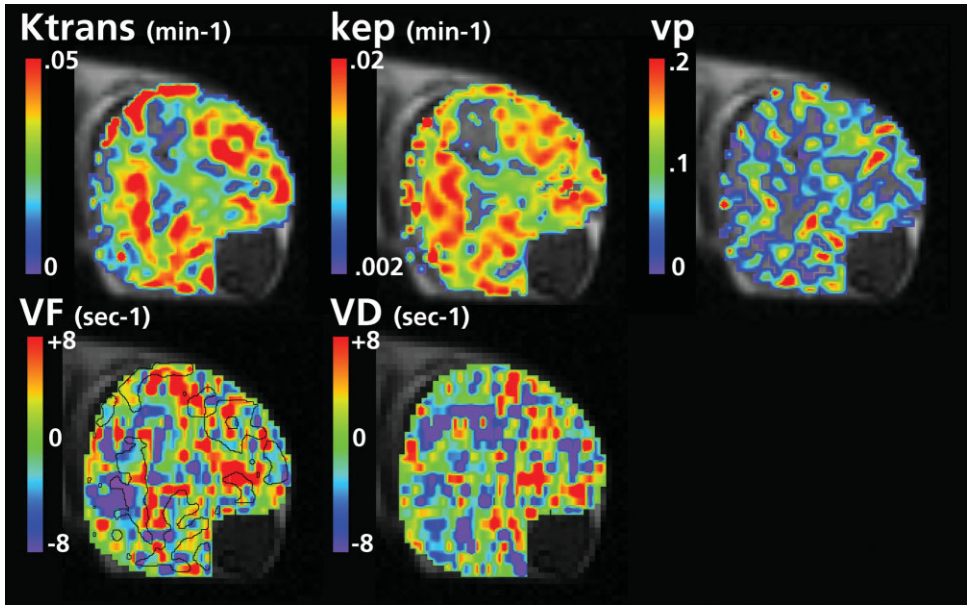

FIG. 6. Typical example of DCE-MRI (top line) and BOLD-MRI (bottom line) parameter maps in an FSa-II tumor. Contour lines of hot spots (red zones) of $K^{Trans}{}_{in}$ are superimposed on the VF map. Note the discordance of spatial distribution between the DCE and BOLD parameters.

revealed no significant correlation between the mean VF and mean V_p, or between the mean VD and mean V_p (see Table 1). There was a positive correlation between mean tumor V_p and mean significant k_{ep} values ($r^2 = 0.78$, $P = .009$), but no correlation between the mean tumor V_p and mean tumor k_{ep} or $K^{Trans}{}_{in}$. In addition, the mean tumor V_p and the fraction of perfused (i.e., with contrast-agent entry) tumor were inversely correlated ($r^2 = 0.74$, $P = .01$; Table 1). On a voxel-by-voxel basis, a positive correlation was found consistently (6/7 tumors) between VF and V_p, but the degree to which parameters were associated was low (individual $r^2 = 0.02–0.14$).

DISCUSSION

In the present study we compared DCE-MRI parameters (macromolecular Gd contrast agent) with BOLD-derived parameters (during hypercapnia and carbogen) representing vessel maturation and function. In this work we attempted to answer the following questions:

Is Vessel Maturity As Revealed by BOLD-MRI Correlated With Contrast Agent Uptake (or Efflux)?

In this study the vasculature in FSa-II fibrosarcoma tumor was revealed to be largely immature. This is consistent with previously obtained immunohistological data (27). Most (78%) of the mature tumor regions showed contrast agent influx, which is consistent with the concept that only functional vessels will demonstrate BOLD contrast change upon hypercapnia.

The physiologic interpretation for $K^{Trans}{}_{in}$ is that it reflects capillary permeability, assuming that blood flow is sufficient (25). The classic view concerning tumor vasculature is that immature vessels are typically hyperpermeable (30). In this study we observed that normal muscle, which is assumed to be made up of mature vessels, exhibited lower values of $K^{Trans}{}_{in}$ (slower and poorer contrast enhancement) than in intramuscularly implanted FSa tumors. This would reflect the selective hyperpermeability of tumor vessels. We also compared $K^{Trans}{}_{in}$ (significant values only) between mature and immature tumor regions. However, there was no systematic evidence of higher values of $K^{Trans}{}_{in}$ for immature vs. mature regions in the tumor tissue. Since P792 is an intermediate-sized contrast agent (~10× larger than Gd-DTPA but ~10× smaller than albumin-Gd-DTPA), it is still unclear whether the pharmacokinetics of this agent are governed by permeability or by blood flow. The use of a macromolecular contrast agent, such as albumin Gd-DTPA, may have better differentiated the two tumor regions (31). However, there is also evidence in the literature that there can be a lack of correlation between maturation and reduced permeability. For example, Gilad et al. (16) observed that a third of all mature vessels were hyperpermeable to albumin Gd-DTPA in the rim of human ovarian carcinoma cells.

We also quantified the relationship between VD (intensity of BOLD response to hypercapnia) and $K^{Trans}{}_{in}$ or k_{ep}. There was no evidence of a strong correlation between these parameters, apart from a nearly significant positive correlation between mean VD and k_{ep} across tumors. Correlations were stronger when VF (the intensity of the BOLD response to carbogen) and k_{ep} were compared, as discussed below.

The lack of evidence of correlation with contrast-media uptake may also be attributed to the nonspecificity of the BOLD-MRI approach. Indeed, a signal change may be observed distal to the site of vessel tone modulation as the result of serial redistribution of blood flow in the tumor. However, the extent of this phenomenon should not be critical for the evaluation of maturity, since we still observed a small fraction of tumor tissue with significant VD, which corroborated our previous histological findings (27). Furthermore, if the same phenomenon occurred during carbogen inhalation, it would not provide a biased measurement of functionality. Estimation of vessel functionality would in fact be even more correlated to the

DCE-MRI measurement. Indeed, the unspecific redistribution of blood flow would occur exclusively in perfused vessels, with or without erythrocytes, but at least with plasma (also allowing contrast-agent arrival). As discussed further below, we observed that DCE-MRI marked significantly more perfused vessels compared to BOLD-MRI. This suggests that unspecific redistribution does not play an essential role in evaluations of functionality using the BOLD approach.

How Is Vascular Function, As Assessed Using BOLD-MRI, Correlated With Contrast Agent Uptake?

Assessment of the BOLD response to carbogen breathing has proved to be useful for probing tumor vascular function (18,26,32,33). Tumor vascular function can also be assessed with the use of DCE-MRI. In this study we observed that DCE-MRI systematically gave higher estimates of the percentage of functional tumor region than BOLD-MRI. The discrepancy between the two techniques may be explained by the poor intrinsic contrast sensitivity of BOLD-MRI in tumor vessels with low hematocrit, relative to DCE-MRI (the contrast-agent influx in the blood stream of the vessel is unaffected by hematocrit) (18). Another possible explanation relates to the generally lower sensitivity of BOLD-MRI. Indeed, each technique is limited by its detection limit. For example, in our study the lowest significant value for VF that the method could detect among tumor voxels was 1.2 s^{-1}, whereas for V_p it was 0.99%, and for $K^{Trans}{}_{in}$ it was 0.002 min^{-1}. Conventional GRE BOLD imaging with a long TE or train of TEs may not be sensitive enough to detect all changes in T_2^* that reflect changes in blood oxygenation. al Hallaq et al. (34) and Foxley et al. (35) demonstrated that a loss of sensitivity is observed when the water resonance does not behave as a homogeneous broadened Lorentzian line. With high-resolution echo-planar spectroscopic imaging (EPSI), the analysis of changes in individual Fourier components of the water resonance during carbogen breathing could reveal BOLD changes that were missed by conventional imaging. It was beyond the scope of this study to determine whether BOLD imaging using EPSI correlates better with DCE-MRI, and this issue warrants further investigation.

How Is the Magnitude of the BOLD Signal Change During Carbogen Challenge Correlated With Contrast Agent Uptake (or Efflux) and Plasma Volume?

The BOLD response to carbogen depends on several parameters, such as the basal blood oxygen level, vessel density, and hematocrit, all of which are related to the level of tissue hypoxia. A recent paper dealt with the dominant role of regional blood vessel density in determining the size of the BOLD response (26). Accordingly, we found it reasonable to postulate that in tumor regions with high intensity of BOLD signal changes, higher values of $K^{Trans}{}_{in}$ or V_p would be observed, presuming that in such regions sustained angiogenesis would have occurred. However, in this study we did not clearly observe any such relationships. The lack of evidence of correlation was not due to noisy data. Figure 6 clearly shows that the spatial distribution of zones of high VF values (associated with high SNR) did not overlap with zones of high $K^{Trans}{}_{in}$ values (i.e., voxels with large contrast enhancement and hence a high SNR).

Intratumoral correlations between VF and V_p were very weak (at most, 14% of the variance of VF could be explained by V_p). Errors in V_p estimation could have accounted for the lack of correlation with VF. However, the Gd contrast agent we used (P792) can provide reliable assessment of blood plasma volume due to lower transendothelial diffusion (compared to Gd-DTPA) (31,36). Intrinsically, VF and V_p are related to blood volume. However, VF is also affected by blood oxygenation change and hematocrit. Furthermore, conversion of V_p to blood volume requires hematocrit data. Discrepancies between local hematocrit and fractional plasma volume in tumor microvessels could account for the poor relationship between VF and V_p (37).

Interestingly, VF and k_{ep} correlated only when averaged over the whole tumor. Thus, tumors that showed lower values of k_{ep} were associated with limited BOLD carbogen responsiveness. The weak net global BOLD response in such tumors was due to the presence of negative BOLD changes during carbogen breathing and hypercapnia. It has been demonstrated that positive changes observed during hypercapnia are due to a decrease in apparent T_1 via the inflow effect (increase in tissue perfusion) (14). Positive changes during carbogen breathing are due to both increased inflow (T_1 effect) and increased blood oxygenation (increase in R_2^*) (10). Although negative changes during a gas-breathing challenge were previously reported by us as well as others (8,11,38), our understanding of this phenomenon and its relevance is still currently limited. Areas of reduced signal were observed following a local increase in blood volume. Vasodilatory effects of CO_2 can result in a net increase in R_2^*. Negative changes may also result from the so-called "steal effect," which occurs when a local large blood flow increase "steals" blood flow from other areas of the tumor (39).

The positive correlation between VF and k_{ep} we observed seems to contradict results reported by Rijpkema et al. (22), who reported that changes in T_2^* correlated inversely with k_{ep}. In their study, mean k_{ep} values were computed for Gd-DTPA-enhancing pixels only. When k_{ep} is estimated from an ROI encompassing a whole tumor, a small value can mean that either the tumor-perfused fraction is small (i.e., many voxels with a value of zero for k_{ep}) or there is a reduction in efflux (low values for k_{ep} in perfused tumor regions). It is not possible to discriminate between the two phenomena. The fact that in our study there was no correlation between the mean k_{ep} over perfused tumor regions and the mean VF over carbogen-responsive or mean tumor ($r = +0.30$, $P = .50$; $r = +0.33$, $P = .47$, respectively) implies that the inclusion of tumor pixels with no blood flow (by using a whole-tumor ROI) created an artifactual correlation between mean tumor k_{ep} and VF. Such a correlation merely demonstrates that the less the tumor is perfused (in terms of percentage of the perfused tumor area), the less it has the capacity to respond to carbogen breathing (in terms of an increase in the BOLD signal).

In conclusion, characterizations of tumor microvasculature using BOLD- and DCE-MRI techniques appear to be largely complementary, given the weak correlations between their corresponding derived parameters (VD and VF

for BOLD-MRI, and V_p, $K^{Trans}{}_{in}$, and k_{ep} for DCE-MRI). Their relevance in terms of predicting treatment outcome and prognosis remain unclear and should be investigated in future studies.

REFERENCES

1. Ogawa S, Lee TM. Magnetic resonance imaging of blood vessels at high fields: in vivo and in vitro measurements and image simulation. Magn Reson Med 1990;16:9–18.
2. Baudelet C, Gallez B. Current issues in the utility of blood oxygen level dependent (BOLD) MRI for the assessment of modulations in tumor oxygenation. Curr Med Imaging Rev 2005;1:229–243.
3. Choyke PL, Dwyer AJ, Knopp MV. Functional tumor imaging with dynamic contrast-enhanced magnetic resonance imaging. J Magn Reson Imaging 2003;17:509–520.
4. Abramovitch R, Itzik A, Harel H, Nagler A, Vlodavsky I, Siegal T. Halofuginone inhibits angiogenesis and growth in implanted metastatic rat brain tumor model—an MRI study. Neoplasia 2004;6:480–489.
5. Hou H, Khan N, O'Hara JA, Grinberg OY, Dunn JF, Abajian MA, Wilmot CM, Makki M, Demidenko E, Lu SY, Steffen RP, Swartz HM. Effect of RSR13, an allosteric hemoglobin modifier, on oxygenation in murine tumors: an in vivo electron paramagnetic resonance oximetry and BOLD-MRI study. Int J Radiat Oncol Biol Phys 2004;59:834–843.
6. Rijpkema M, Kaanders JH, Joosten FB, van der Kogel AJ, Heerschap A. Effects of breathing a hyperoxic hypercapnic gas mixture on blood oxygenation and vascularity of head-and-neck tumors as measured by magnetic resonance imaging. Int J Radiat Oncol Biol Phys 2002;53: 1185–1191.
7. Thomas CD, Chenu E, Walczak C, Plessis MJ, Perin F, Volk A. Relationship between tumour growth rate and carbogen-based functional MRI for a chemically induced HCC in mice. MAGMA 2004;17:271–280.
8. Baudelet C, Gallez B. Cluster analysis of BOLD fMRI time series in tumors to study the heterogeneity of hemodynamic response to treatment. Magn Reson Med 2003;49:985–990.
9. Gross S, Gilead A, Scherz A, Neeman M, Salomon Y. Monitoring photodynamic therapy of solid tumors online by BOLD-contrast MRI. Nat Med 2003;9:1327–1331.
10. Howe FA, Robinson SP, McIntyre DJ, Stubbs M, Griffiths JR. Issues in flow and oxygenation dependent contrast (FLOOD) imaging of tumours. NMR Biomed 2001;14:497–506.
11. Kuperman VY, River JN, Lewis MZ, Lubich LM, Karczmar GS. Changes in T2*-weighted images during hyperoxia differentiate tumors from normal tissue. Magn Reson Med 1995;33:318–325.
12. Jordan BF, Misson P, Demeure R, Baudelet C, Beghein N, Gallez B. Changes in tumor oxygenation/perfusion induced by the no donor, isosorbide dinitrate, in comparison with carbogen: monitoring by EPR and MRI. Int J Radiat Oncol Biol Phys 2000;48:565–570.
13. Baudelet C, Ansiaux R, Jordan BF, Havaux X, Macq B, Gallez B. Physiological noise in murine solid tumours using T2*-weighted gradient-echo imaging: a marker of tumour acute hypoxia? Phys Med Biol 2004;49:3389–3411.
14. Neeman M, Dafni H, Bukhari O, Braun RD, Dewhirst MW. In vivo BOLD contrast MRI mapping of subcutaneous vascular function and maturation: validation by intravital microscopy. Magn Reson Med 2001;45:887–898.
15. Gilead A, Meir G, Neeman M. The role of angiogenesis, vascular maturation, regression and stroma infiltration in dormancy and growth of implanted MLS ovarian carcinoma spheroids. Int J Cancer 2004;108: 524–531.
16. Gilad AA, Israely T, Dafni H, Meir G, Cohen B, Neeman M. Functional and molecular mapping of uncoupling between vascular permeability and loss of vascular maturation in ovarian carcinoma xenografts: The role of stroma cells in tumor angiogenesis. Int J Cancer 2005;117:202–211.
17. Abramovitch R, Dafni H, Smouha E, Benjamin LE, Neeman M. In vivo prediction of vascular susceptibility to vascular susceptibility endothelial growth factor withdrawal: magnetic resonance imaging of C6 rat glioma in nude mice. Cancer Res 1999;59:5012–5016.
18. Robinson SP, Rijken PF, Howe FA, McSheehy PM, van der Sanden BP, Heerschap A, Stubbs M, van der Kogel AJ, Griffiths JR. Tumor vascular architecture and function evaluated by non-invasive susceptibility MRI methods and immunohistochemistry. J Magn Reson Imaging 2003;17: 445–454.
19. Robinson SP, Collingridge DR, Howe FA, Rodrigues LM, Chaplin DJ, Griffiths JR. Tumour response to hypercapnia and hyperoxia monitored by FLOOD magnetic resonance imaging. NMR Biomed 1999;12:98–106.
20. Padhani AR, Husband JE. Dynamic contrast-enhanced MRI studies in oncology with an emphasis on quantification, validation and human studies. Clin Radiol 2001;56:607–620.
21. Padhani AR. Dynamic contrast-enhanced MRI in clinical oncology: current status and future directions. J Magn Reson Imaging 2002;16: 407–422.
22. Rijpkema M, Schuuring J, Bernsen PL, Bernsen HJ, Kaanders JH, van der Kogel AJ, Heerschap A. BOLD-MRI response to hypercapnic hyperoxia in patients with meningiomas: correlation with gadolinium-DTPA uptake rate. Magn Reson Imaging 2004;22:761–767.
23. Jiang L, Zhao D, Constantinescu A, Mason RP. Comparison of BOLD contrast and Gd-DTPA dynamic contrast-enhanced imaging in rat prostate tumor. Magn Reson Med 2004;51:953–960.
24. Peller M, Weissfloch L, Stehling MK, Weber J, Bruening R, Senekowitsch-Schmidtke R, Molls M, Reiser M. Oxygen-induced MR signal changes in murine tumors. Magn Reson Imaging 1998;16:799–809.
25. Tofts PS, Brix G, Buckley DL, Evelhoch JL, Henderson E, Knopp MV, Larsson HB, Lee TY, Mayr NA, Parker GJ, Port RE, Taylor J, Weisskoff RM. Estimating kinetic parameters from dynamic contrast-enhanced T(1)-weighted MRI of a diffusable tracer: standardized quantities and symbols. J Magn Reson Imaging 1999;10:223–232.
26. Rodrigues LM, Howe FA, Griffiths JR, Robinson SP. Tumor R2* is a prognostic indicator of acute radiotherapeutic response in rodent tumors. J Magn Reson Imaging 2004;19:482–488.
27. Baudelet C, Cron GO, Ansiaux R, Crokart N, Dewever J, Feron O, Gallez B. The role of vessel maturation and vessel functionality in spontaneous fluctuations of T(2)*-weighted GRE signal within tumors. NMR Biomed 2006;19:69–76.
28. Fan X, Medved M, River JN, Zamora M, Corot C, Robert P, Bourrinet P, Lipton M, Culp RM, Karczmar GS. New model for analysis of dynamic contrast-enhanced MRI data distinguishes metastatic from nonmetastatic transplanted rodent prostate tumors. Magn Reson Med 2004;51: 487–494.
29. Friston KJ, Holmes AP, Poline JB, Grasby PJ, Williams SC, Frackowiak RS, Turner R. Analysis of fMRI time-series revisited. Neuroimage 1995; 2:45–53.
30. Dvorak HF. Angiogenesis: update 2005. J Thromb Haemost 2005;3: 1835–1842.
31. Turetschek K, Floyd E, Shames DM, Roberts TP, Preda A, Novikov V, Corot C, Carter WO, Brasch RC. Assessment of a rapid clearance blood pool MR contrast medium (P792) for assays of microvascular characteristics in experimental breast tumors with correlations to histopathology. Magn Reson Med 2001;45:880–886.
32. Baudelet C, Gallez B. How does blood oxygen level-dependent (BOLD) contrast correlate with oxygen partial pressure (pO2) inside tumors? Magn Reson Med 2002;48:980–986.
33. Fan X, River JN, Zamora M, al Hallaq HA, Karczmar GS. Effect of carbogen on tumor oxygenation: combined fluorine-19 and proton MRI measurements. Int J Radiat Oncol Biol Phys 2002;54:1202–1209.
34. al Hallaq HA, Fan X, Zamora M, River JN, Moulder JE, Karczmar GS. Spectrally inhomogeneous BOLD contrast changes detected in rodent tumors with high spectral and spatial resolution MRI. NMR Biomed 2002;15:28–36.
35. Foxley S, Yang C, Fan X, Zamora M, Panti R, River JN, Karczmar GS. The use of high spatial and spectral resolution Fourier component difference images to detect BOLD response in mouse tumors [Abstract]. In: Proceedings of the 13th Annual Meeting of ISMRM, Miami Beach, FL, USA, 2005. p 2108.
36. Ruehm SG, Christina H, Violas X, Corot C, Debatin JF. MR angiography with a new rapid-clearance blood pool agent: Initial experience in rabbits. Magn Reson Med 2002;48:844–851.
37. Dewhirst MW. Concepts of oxygen transport at the microcirculatory level. Semin Radiat Oncol 1998;8:143–150.
38. Griffiths JR, Taylor NJ, Howe FA, Saunders MI, Robinson SP, Hoskin PJ, Powell ME, Thoumine M, Caine LA, Baddeley H. The response of human tumors to carbogen breathing, monitored by gradient-recalled echo magnetic resonance imaging. Int J Radiat Oncol Biol Phys 1997; 39:697–701.
39. Zlotecki RA, Baxter LT, Boucher Y, Jain RK. Pharmacologic modification of tumor blood flow and interstitial fluid pressure in a human tumor xenograft: network analysis and mechanistic interpretation. Microvasc Res 1995;50:429–443.